Journal of Pathology
J Pathol 2012; **228:** 416–428
Published online in Wiley Online Library
(wileyonlinelibrary.com) DOI: 10.1002/path.4077

ORIGINAL PAPER

Synergistic regulation of p53 by Mdm2 and Mdm4 is critical in cardiac endocardial cushion morphogenesis during heart development

Qin Zhang,[1,2] Xueyan He,[1] Lai Chen,[1] Chenxi Zhang,[1] Xiang Gao,[1] Zhongzhou Yang[1] and Geng Liu[1]*

[1] *The MOE Key Laboratory of Model Animal for Disease Study and the Model Animal Research Center, Nanjing University, Nanjing, China*
[2] *Institute of Biophysics, Chinese Academy of Sciences, Beijing, China*

**Correspondence to: Geng Liu, The MOE Key Laboratory of Model Animal for Disease Study and the Model Animal Research Center, Nanjing University, Nanjing, China. e-mail: liugeng@nicemice.cn*

Abstract

Congenital heart defects (CHDs) are the most prevalent human birth defects. More than 85% of CHDs are thought to result from a combination of genetic susceptibilities and environmental stress. However, the stress-related signalling pathways involved remain largely unknown. The p53 transcription factor is a key tumour suppressor and a central regulator of the cellular stress responses. p53 activities are tightly regulated by its inhibitors Mdm2 and Mdm4 at the post-translational level. Here we used the Cre–loxP system to delete *Mdm2* (*Tie2Cre;Mdm2*$^{FM/FM}$) or one copy of both *Mdm2* and *Mdm4* (*Tie2Cre;Mdm2*$^{FM/+}$*; Mdm4*$^{+/-}$) in endothelial/endocardial cells and their derivatives in mice to examine the regulation of the p53/Mdm2–Mdm4 pathway during vascular and cardiovascular development. The *Tie2Cre;Mdm2*$^{FM/FM}$ mice died before embryonic day 10.5 (E10.5) and displayed severe vascular defects. On the other hand, the *Tie2Cre;Mdm2*$^{FM/+}$*; Mdm4*$^{+/-}$ mice displayed atrial and ventricular septal defects (ASD, VSD) of the heart, leading to severe heart dysfunction and postnatal death. During cardiac endocardial cushion morphogenesis, p53 activation was associated with defects in both the epithelial–mesenchymal transition (EMT) of the endocardial cells and the post-EMT proliferation of the mesenchymal cells, and the valvuloseptal phenotypes of the *Tie2Cre;Mdm2*$^{FM/+}$*; Mdm4*$^{+/-}$ mice were fully rescued by deletion of one copy of p53. Strikingly, maternal exposure to low-dose X-rays in *C57BL/6* mice mimicked the congenital heart malformations seen in the *Tie2Cre;Mdm2*$^{FM/+}$*; Mdm4*$^{+/-}$ model, which was also dependent on p53 status, establishing a link between maternal exposures and CHD susceptibility through the p53 pathway. These data revealed a new regulatory mechanism in cardiac endocardial cushion morphogenesis and suggested a possible cause of CHDs due to environmental stress.

Keywords: p53; congenital heart defects; vasculogenesis; endocardial cushion morphogenesis; EMT

Received 15 February 2012; Revised 8 July 2012; Accepted 11 July 2012

No conflicts of interest were declared.

Introduction

The p53 transcription factor is a central regulator of the cellular stress responses [1]. p53 and its isoforms are highly expressed during early development in mammals [2], and the precise balance of p53 activity is necessary for correct embryonic development [3]. The expression and activity of p53 are monitored by many layers of regulation, mainly at the post-translational level by Mdm2 and Mdm4 [4,5]. Mdm2 functions as an E3 ubiquitin ligase responsible for the ubiquitination and degradation of p53 [6,7]. In response to many forms of stresses, the association between p53 and Mdm2 is disrupted, leading to p53 stabilization and activation [5,8]. Mdm4, a homologue of Mdm2, appears to inhibit p53 by masking its transcriptional activation domain [9]. Genetic deletion of either *Mdm2* or *Mdm4* in mice yields embryonic lethal phenotypes that are fully rescued by deletion of p53 [5]. Tissue-specific deletion of *Mdm2* in either neural progenitor cells or cardiomyocytes results in embryonic lethality, whereas deletion of *Mdm4* in the same lineages results in a milder tissue defect or live birth [10–13]. In support of their non-overlapping and synergistic roles in inhibiting p53, constitutive *Mdm2* and *Mdm4* haploinsufficiency leads to increased p53 activity and embryonic lethality [14].

Congenital heart defects (CHDs) are the most frequent form of birth defects in humans, present in about 1% of all live births [15,16]. Mortality from CHDs remains a major cause of death in infancy and childhood [17]. Cardiac malformations attributable to aberrant development of the atrioventricular valvuloseptal complex are among the most common forms of CHDs [18,19]. During early vertebrate heart development, the formation of atrioventricular (AV) cushions

is an important step in valvuloseptal development to form the four-chambered heart, while a vital event in endocardial cushion morphogenesis is epithelial-to-mesenchymal transition (EMT), where specific endocardial cells in the endocardium surrounding the cardiac cushions are activated to delaminate from the endocardial layer, transform into mesenchyme, and migrate into the underlying extracellular matrix [20]. Further proliferation and remodelling of these mesenchymal cells as well as the extracellular matrix result in the formation of membranous portions of the atrial and ventricular septae, and the generation of thin, pliable valves, creating the partitioned four-chamber heart [20,21].

More than 85% of CHDs are thought to result from a complex interaction between maternal exposures and fetal genetic susceptibilities [22–25]. However, these epidemiological studies have mostly suggested risk rather than pinpointing the underlying disease mechanisms. Endocardial cushion morphogenesis, especially the EMT and post-EMT remodelling events, is influenced by many signalling pathways [26], but the stress-induced signalling pathways involved remain largely unknown. In this study, the roles of p53/Mdm2–Mdm4 pathway regulation during mouse cardiac endocardial cushion morphogenesis and its involvement in stress-induced heart malformation in mice were investigated.

Materials and methods

Mice and the breeding strategy

The *R26RstoplacZ (Rosa26)* [27], $p53^{+/-}$ [28], and *Tie2 Cre* mice [29] were obtained from the Model Animal Research Center of Nanjing University. Mice with $Mdm2^{FM}$ [30] and *Mdm4* [10,12] alleles have been described previously. The experimental animal facility has been accredited by the AAALAC (Association for Assessment and Accreditation of Laboratory Animal Care International), and the IACUC (Institutional Animal Care and Use Committee) of the Model Animal Research Institute of Nanjing University approved all animal protocols used in this study. To generate the *Tie2Cre;*$Mdm2^{FM/FM}$ mice, $Mdm2^{FM/FM}$ females were bred with *Tie2Cre;*$Mdm2^{FM/+}$ males. All littermates were used as controls in the *Tie2Cre;*$Mdm2^{FM/FM}$ study. To generate the *Tie2Cre;* $Mdm2^{FM/+}$; $Mdm4^{+/-}$ mice, $Mdm2^{FM/FM}$ females were bred with *Tie2Cre;*$Mdm4^{+/-}$ males. The littermates from this cross except for the *Tie2Cre;* $Mdm2^{FM/+}$ genotype were used as controls.

Immunofluorescence (IF) staining

Standard protocols and commercially available antibodies were used in most instances to whole mount stained and fixed samples, and dewaxed sections. Antigen retrieval was processed by incubating in 0.01 M sodium citrate buffer (pH 6.0) for 25 min in a steamer. Cell proliferation was analysed using the BrdU incorporation assay (Upstate, Lake Placid, NY, USA). Confocal images were obtained with Olympus TM FluoView 1000 and Leica TCS SP5 Microsystems. Antibodies to fibronectin (610 078), β-catenin (610 153), and PECAM (557 355) were from BD Biosciences (San José, CA, USA). Vimentin (SC-5565) was from Santa Cruz Biotechnology (Santa Cruz, CA, USA). Endomucin (14-5851-85) was from eBioscience (San Diego, CA, USA). p-p53 (ser15, 9284) was from CST (Cell Signaling Technology, Beverly, MA, USA). p21 (RB-032-p1) was from NeoMarkers (Flemont, CA, USA).

LacZ staining

Whole-mount lacZ staining of embryos was performed as described previously [29]. Whole-mount stained embryos were then embedded in paraffin, sectioned at 7 mm, and mounted on the slides. LacZ-stained sections were lightly counterstained with eosin, mounted, and photographed under an Olympus DP70 microscope.

Quantitative (Q)-PCR analysis

RNA was isolated from the heart tubes of embryos either at the E8.5–E9.0 stage or at E9.5 with TRIzol (Invitrogen, Carlsbad, CA, USA). Reverse transcription reactions were accomplished using a Reverse Transcription System (Promega, Madison, WI, USA). Primers for Q-PCR are described in Supplementary Table 1. Q-PCRs were performed with Light Cycler SYBR green DNA master mix (Takara, Dalian, China) on an ABI7300 thermal cycler in triplicate. The specificity of Q-PCR was confirmed by melting curves of each PCR product. Data were expressed as cycle threshold (Ct) and used to determine ΔCt (dCt) values. The fold difference in gene expression between

Table 1. Cardiovascular phenotypes in the *Tie2Cre;* $Mdm2^{FM/+}$; $Mdm4^{+/-}$ mice

Age	Genotype	Total	Abnormal	ASD	VSD	AVSD	Other phenotypes†
E14.5	Control	10	2 (20%)	2 (20%)	0	0	0
	Tie2CreMM	8	8 (100%)**	2 (25%)	1 (12.5%)	5 (62.5%)	0
P1	Control	14	3 (21.4%)	2 (14.3 %)	0	0	1 (7.1%)
	Tie2CreMM	10	7 (70%)*	4 (40%)	0 (0%)	1 (10%)	2 (20%)
∼P15	Control	13	1 (7.6%)	0	0	0	1 (7.6%)
	Tie2CreMM	15	11 (73.3%)**	5 (33.3%)	2 (13.3%)	1 (6.6%)	3 (20%)

†Included DORV (double-outlet right ventricle), valve hypertrophy, and abnormally large blood vessels in the ventricular septum. Numbers in parentheses indicate the percentage of mice affected in the group. Asterisks indicate significant differences between the mutant and control mice (*$p < 0.05$, **$p < 0.01$).

control and mutant samples was calculated as follows: fold difference $= 2^{-\text{difference in dCt}}$.

AV canal explant assay

The AV canal explant assay was performed essentially as described previously [31]. Nutlin-3 (Roche, Nutley, NJ, USA) was added as a supplement to the complete media when necessary. After 48 h, explants were fixed with 4% PFA and stained with 0.2 unit/ml of Alexa Fluor 488 Phalloidin (Invitrogen) and TOPRO-3 (Invitrogen). There were no differences between wild-type and mutant explants in terms of attachment and survival rates. Confocal laser scanning microscopy was performed using the Olympus FluoView 1000.

Echocardiography

Echocardiography was performed with Vevo770 (Visual Sonics, Toronto, Canada) using a single-element mechanical transducer with a centre frequency of 30 MHz. Each mouse was scanned with two-dimensional (2D) imaging and Doppler imaging in parasternal long-axis, short-axis, and apical four-chamber views. The frame rate in 2D imaging was set as 50–60 Hz, with the focal length at 12.5–12.7 mm.

Surface ECG

Electrocardiogram (ECG) in lead II was continuously monitored and recorded using a data acquisition system (Power Lab 8/30, AD Instruments, Bella Vista, NSW, Australia). The surface ECG tracings were filtered using a high-pass setting of 0.3 Hz and a low-pass setting of 1 kHz. The ECG parameters were evaluated by Lab Chart 6 software (AD Instruments) following standard criteria: (i) the heart rate (beats per minute) was monitored, and (ii) the variation at P wave and the PQ, QRS, and QT intervals were measured in milliseconds.

X-irradiation

The timed pregnant mice were exposed to whole-body X-ray irradiation by a single dose of 0.3 Gy. The animals were kept in a cardboard cage encompassed by the radiation field and were allowed to move freely in the cage during irradiation. An XHA600C Medical Linear Accelerator (Xinhua Medical Equipments Co Ltd, Shandong, China) was used.

Statistical analysis

Data are presented as the mean ± SEM. Statistical analyses were performed using the two-tailed Student's t-test for parametric data and Pearson's chi-squared test (χ^2) for categorical data. $p < 0.05$ ($*$) was considered statistically significant and $p < 0.01$ ($**$) statistically highly significant.

Results

Loss of Mdm2 in the endothelium results in embryonic lethality

Endothelial-specific *Tie2-Cre* transgenic mice provide a valuable tool to study the roles of molecules involved in the development of vasculature and in epithelial–mesenchymal transformation during heart endocardial cushion morphogenesis *in vivo* [29]. To determine whether Mdm2 is required during vasculogenesis and endocardial cushion morphogenesis, female mice with an *Mdm2* conditional allele ($Mdm2^{FM}$) [30] were mated to male *Tie2Cre* transgenic mice to generate $Tie2Cre;Mdm2^{FM/+}$ and $Tie2Cre;Mdm2^{FM/FM}$ mice. Some of these mice were also generated in a *Rosa 26* background to depict the endothelial lineage. The $Tie2Cre;Mdm2^{FM/+}$ mice were normal, but no homozygous pups were obtained from the $Tie2Cre;Mdm2^{FM/+} \times Mdm2^{FM/FM}$ crosses. Further genotypic and phenotypic analyses at various stages post-conception (Supplementary Table 2) revealed that

Table 2. Echocardiographic parameters of $Tie2Cre;Mdm2^{FM/+};Mdm4^{+/-}$ mice and their littermates

	P1		P10		P21	
	Control ($n = 8$)	*Tie2CreMM* ($n = 6$)	Control ($n = 7$)	*Tie2CreMM* ($n = 5$)	Control ($n = 10$)	*Tie2CreMM* ($n = 11$)
IVS;d (mm)	0.27 ± 0.04	0.23 ± 0.05	0.46 ± 0.12	0.40 ± 0.11	0.60 ± 0.08	0.54 ± 0.09
LVID;d (mm)	1.21 ± 0.13	1.28 ± 0.20	2.02 ± 0.25	1.89 ± 0.21	2.53 ± 0.44	2.69 ± 0.45
LVPW;d (mm)	0.34 ± 0.08	0.36 ± 0.07	0.45 ± 0.06	0.47 ± 0.13	0.72 ± 0.09	0.69 ± 0.11
IVS;s (mm)	0.44 ± 0.09	0.39 ± 0.08	0.62 ± 0.13	0.59 ± 0.09	0.82 ± 0.11	0.78 ± 0.14
LVID;s (mm)	0.76 ± 0.12	0.72 ± 0.11	1.13 ± 0.19	1.16 ± 0.26	1.46 ± 0.10	1.56 ± 0.14
LVPW;s (mm)	0.39 ± 0.08	0.37 ± 0.07	0.67 ± 0.11	0.68 ± 0.11	0.92 ± 0.18	0.94 ± 0.23
LV Vol;d (mm)	3.52 ± 1.06	3.39 ± 0.93	15.77 ± 0.97	14.86 ± 1.22	24.89 ± 4.86	25.62 ± 3.71
LV Vol;s (mm)	1.06 ± 0.29	0.97 ± 0.25	4.92 ± 0.90	5.20 ± 1.75	7.41 ± 1.18	6.89 ± 1.76
EF (%)	75.6 ± 6.21	70.1 ± 3.78**	84.5 ± 5.32	61.7 ± 8.96*	75.3 ± 4.24	79.0 ± 8.61
FS (%)	40.9 ± 5.58	35.8 ± 2.48*	47.5 ± 6.14	41.3 ± 5.19*	36.2 ± 4.04	42.1 ± 6.70
E/A	0.65 ± 0.20	0.75 ± 0.14	1.55 ± 0.13	1.16 ± 0.23*	1.7 ± 0.18	2.4 ± 0.33*
LV mass (mg)	2.72 ± 0.81	3.03 ± 1.33	18.4 ± 2.88	20.9 ± 3.16	31.5 ± 2.75	25.2 ± 3.92

Transthoracic echocardiography was performed on P1, P10, and P21 *Tie2CreMM* and littermate control mice. Asterisks indicate significant differences between the mutant and control mice ($*p < 0.05$, $**p < 0.01$), suggesting impaired left ventricular and systolic function of the *Tie2CreMM* hearts.

IVS = interventricular septum; LVID = left ventricular internal dimension; LVPW = left ventricular posterior wall thicknesses; LV = left ventricular; EF = ejection fraction; FS = fractional shortening; E/A = ratio of early to late mitral diastolic flow; Vol = volume; d = diastole; s = systole.

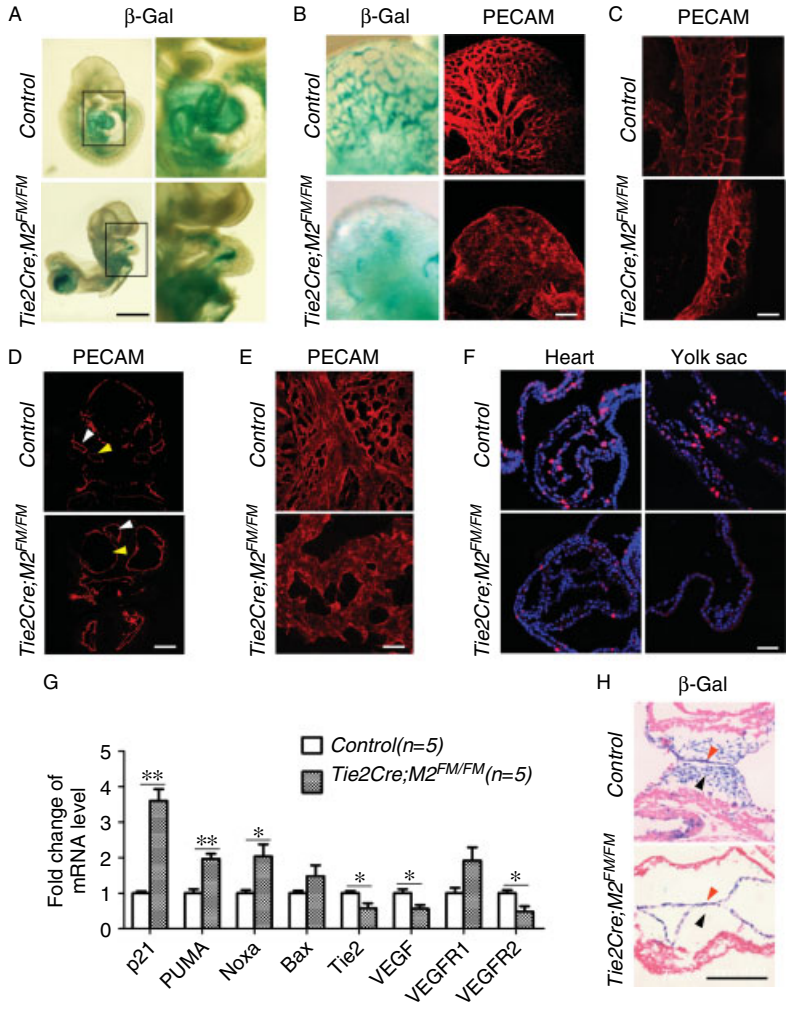

Figure 1. Inactivation of *Mdm2* in endothelial cells leads to embryonic death from severe defects in vascular remodelling. (A) Lateral view of a severely perturbed turning in a *Tie2Cre;Mdm2*$^{FM/FM}$ *Rosa26* embryo (lower panel) compared with the control embryo (upper panel). Higher magnification of the boxed areas shows a normal S-shaped loop of the control heart tube and a special C-shaped loop of the mutant heart tube. Scale bar = 500 μm. (B) Representative images of whole-mount embryos stained with β-Gal and PECAM antibody, illustrating a disorganized pattern of vascular plexus formation and rudimentary vascular network in the head of the mutant embryo compared with the control. Scale bar = 100 μm. (C) Abnormal vascular network in the trunk of the mutant embryo by PECAM whole-mount staining. Scale bar = 100 μm. (D) PECAM immunostaining showing an abnormally enlarged dorsal aorta (yellow arrowhead) and cardinal vein (white arrowhead) in the anterior part of the mutant embryo. Scale bar = 100 μm. (E) PECAM whole-mount staining of yolk sacs. Note the abnormally enlarged vessels with less branching in the mutant and the well-connected networks in the control yolk sac. Scale bar = 100 μm. (F) Diminished BrdU incorporation (red) in the heart tube and the yolk sac of mutant embryos. Scale bar = 100 μm. (G) Real-time PCR analysis of the expression of p53 target genes and angiogenic genes in E8.5–E9.0 heart tubes. The gene expression was normalized to the expression of GAPDH and is presented as fold change ± SEM ($n = 5$) relative to the control embryos. (H) β-Gal staining (blue) of the endocardial cushion of the E9.5 heart in a *Rosa 26* background. Both the endocardial (red arrowhead) and mesenchymal cells (black arrowhead) in the AV cushion of the control embryo were positive for β-Gal staining. Note the relatively intact endocardium (red arrowhead) and the complete absence of endocardium-derived cushion mesenchyme (black arrowhead) in the mutant AV canal. Scale bar = 100 μm.

all the *Tie2Cre;Mdm2*$^{FM/FM}$ embryos showed an abnormal phenotype compared with the control group at embryonic day (E) 9.5 and died at around E10.5.

By E9.5, the *Tie2Cre;Mdm2*$^{FM/FM}$ embryos were growth-retarded, failed to turn, and appeared with a 'C-shaped' looping heart, while the hearts of control embryos had developed into the S-looping stage (Figure 1A). These embryos also displayed severe vascular abnormalities revealed by whole-mount β-Gal staining and PECAM staining, which recognizes the endothelial cell lineage. A strong vascular remodelling defect was shown in head (Figure 1B) and intersomitic (Figure 1C) vessels. Histological analysis also revealed a much enlarged lumen of the dorsal aorta and cardinal veins in the anterior part of the mutant embryo (Figure 1D). The formation of the extraembryonic vasculature in E9.5 mutant embryos was also defective. A dense plexus of small vessels along the large collecting vessels was observed in the control yolk sacs. In contrast, the mutant yolk sacs displayed only irregularly enlarged collecting vessels (Figure 1E). BrdU incorporation indicated that cell cycle arrest was evident in both the endocardium (Figure 1F, left panel) and the yolk sac (Figure 1F, right panel) of the mutant embryo.

Loss of Mdm2 led to p53 activation [5]. To examine the effect of *Mdm2* loss in endothelial cells, real-time PCR was performed on heart tubes of the embryos at about the E8.5–E9.0 stage with representative p53 target genes *p21*, *Noxa*, and *Puma*, as well as major angiogenesis-related factors *VEGF, Tie2, VEGFR1*, and *VEGFR2*. The expression of *p21* and *PUMA* increased significantly in *Tie2Cre;Mdm2*$^{FM/FM}$ heart tube. The levels of pro-angiogenic factor *Tie2, VEGF*, and *VEGFR2* mRNA decreased moderately (Figure 1G).

Tie2Cre;Mdm2$^{FM/+}$*; Mdm4*$^{+/-}$ mice exhibit multiple cardiac defects

Cardiac septum and valve structures are developed first through AV cushion morphogenesis [20]. Cushion mesenchyme is the derivative of the endocardial cells at the cardiac AV canal. Histological examination of the heart showed that both the endocardial and the mesenchymal cells in the AV cushion of the control embryo in a *Rosa 26* background were positive for β-Gal staining, indicating their lineage relationship (Figure 1H). However, *Tie2Cre;Mdm2*$^{FM/FM}$, *Rosa 26* embryos displayed a paucity of mesenchymal cells within the AV cushions, whereas the endocardium in the AV canal of the mutant embryo remained as a normal single cell layer (Figure 1H). The evidence provided the first clue that p53/Mdm2 regulation may be involved in AV endocardial cushion morphogenesis. However, the early lethality of the *Tie2Cre;Mdm2*$^{FM/FM}$ mouse limits the ability to investigate the role of p53 inhibition in this developmental process and subsequent formation of the four-chambered heart. Previous results indicated that *Mdm2* and *Mdm4* have non-overlapping and synergistic roles in inhibiting p53 [14]. We therefore generated mice heterozygous for *Mdm2* in endothelial lineage in the *Mdm4*$^{+/-}$ background (*Tie2Cre;Mdm2*$^{FM/+}$*; Mdm4*$^{+/-}$), referred to as *Tie2CreMM* mice. The recombination of the *Mdm2*^{FM} allele catalysed by Tie2 Cre in these mice was confirmed in the *Rosa26* reporter background (Supplementary Figure 1A) and by genotyping (Supplementary Figure 1B).

The *Tie2CreMM* mice were viable at birth. Unlike the *Tie2Cre;Mdm2*$^{FM/FM}$ embryos, the yolk sac, head, and trunk vascular plexus formation were normal in the *Tie2CreMM* mice (Supplementary Figure 2A). Whole-mount staining of PECAM and Lyve 1, a lymphatic endothelial marker, indicated no obvious defects in either blood or lymphatic vessels of the *Tie2CreMM* skins (Supplementary Figure 2B). Furthermore, the endocardium and the trabeculation of the heart also appeared unaffected in the *Tie2CreMM* mice (Supplementary Figure 2C). However, the majority of these mice died between 1 and 2 weeks of age, and the mortality reached 75% by 3 weeks (Figure 2A). The high mortality of the *Tie2CreMM* mice prompted us to investigate the underlying cause of lethality. Systemic examination revealed no major changes in the haematopoietic system (Supplementary Figure 3), or in the digestive tract, kidney, liver, and lung of the

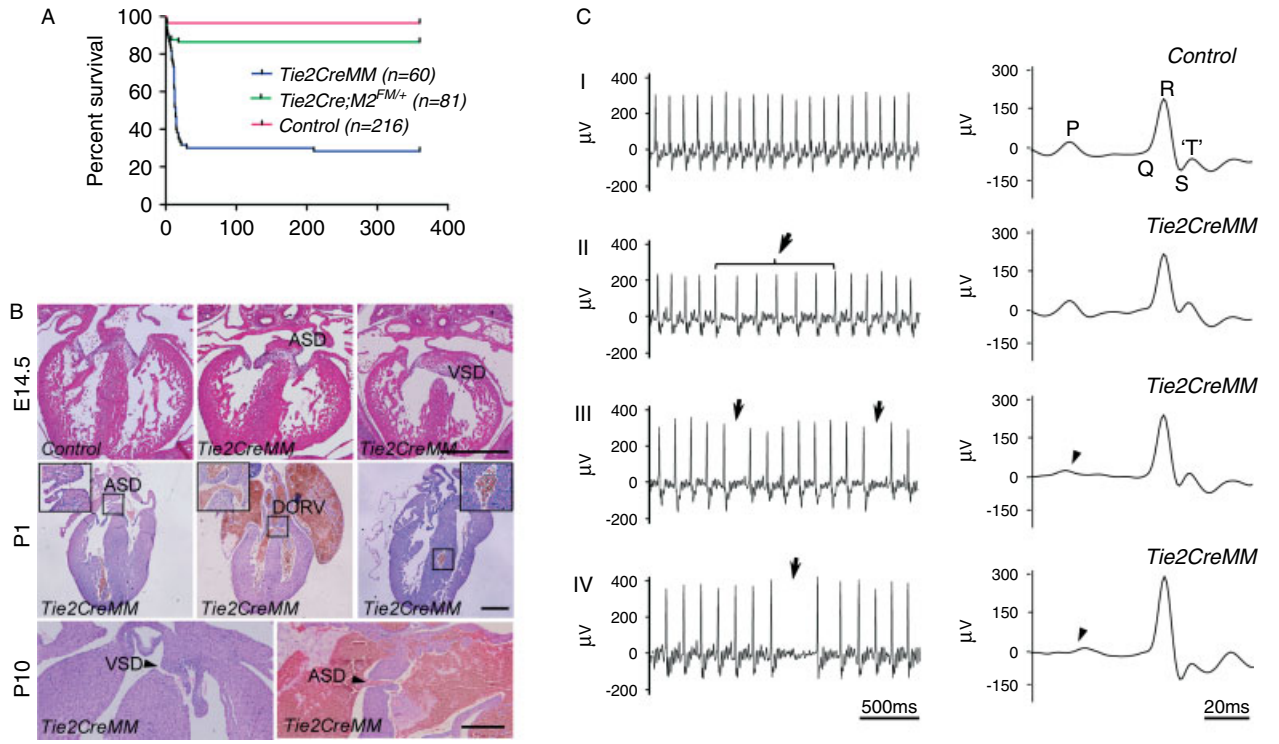

Figure 2. Cardiac valvuloseptal defects and heart dysfunction in *Tie2Cre;Mdm2*$^{FM/+}$*; Mdm4*$^{+/-}$ mice. (A) Kaplan–Meier survival analysis of the *Tie2CreMM* and control mice. (B) Representative cardiac phenotypes of *Tie2CreMM* mice showing VSD, ASD, DORV, and abnormally large blood vessel. Scale bars = 500 μm. (C) Six of 21 surviving *Tie2CreMM* mice exhibited arrhythmias on surface ECG. Representative continuous surface ECG (lead II) recordings from *Tie2CreMM* animals showing sinus arrhythmia (II), escaped rhythm (III), and failure of the sinoatrial node (IV). Arrows indicate arrhythmia and arrowheads indicate the missing p waves.

Tie2CreMM pups (Supplementary Figure 1B). When the heart was closely examined by histological analysis, over 75% (26/33) of the *Tie2CreMM* mice failed to close their atrial or ventricular septum at E14.5 and after (Table 1). Atrial septal defect (ASD), ventricular septal defect (VSD), and hyperplastic valves were commonly found in the *Tie2CreMM* hearts. Double-outlet right ventricle (DORV) and abnormally large blood vessels in the ventricular septum also appeared (Figure 2B).

Severe septum defects and dysplastic valves in the heart chambers often lead to regurgitation of blood and cardiac dysfunction. To evaluate the heart function of the *Tie2CreMM* mice, echocardiography (Echo) was performed at P1, P10, and P21 (Table 2). No significant differences in cardiac diameters and thickness were found in mutant mice compared with the controls, suggesting normal formation of the cardiac wall. However, significant decreases in systolic and diastolic functions were detected in *Tie2CreMM* mice, suggesting specific defects in the septae and valves of these mice.

Abnormal blood flow in the hearts of mice with atrioventricular septal defects may cause heart failure due to arrhythmia, pulmonary hypertension, and blood clots. Six of 21 (28%) surviving *Tie2CreMM* mice with an age range from 2 to 8 weeks exhibited arrhythmias on surface ECG. This abnormality was often due to the junctional escape rhythm or sinus arrhythmia (Figure 2C).

Those findings indicated that *Mdm2* and *Mdm4* haploinsufficiency in endothelium and endocardial cushion impaired atrioventricular valvuloseptal development, leading to heart dysfunctions and postnatal death.

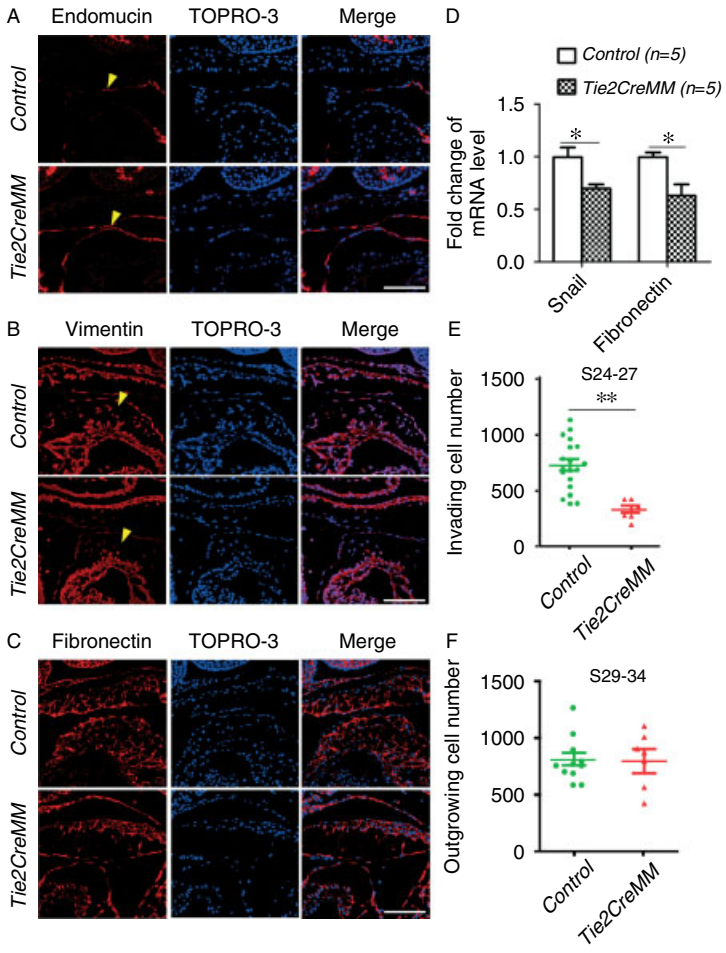

Figure 3. Cardiac endocardial cushion morphogenesis defects in *Tie2Cre;Mdm2*$^{FM/+}$*;Mdm4*$^{+/-}$ mice. (A–C) Immunofluorescence staining of endomucin (A), vimentin (B), and fibronectin (C) of the E9.5 endocardial cushions. Note the retained endomucin expression in *Tie2CreMM* endocardium (arrowheads in A), the reduction of vimentin expression (arrowheads in B), and the diminished deposition of fibronectin in the mutant endocardial cushions. Scale bars = 100 μm. (D) Real-time PCR analysis of the EMT-related gene expression in E9.5 heart tubes. (E) The number of invading mesenchymal cells as a quantitative measurement of the ability of endocardial cells to undergo EMT in the AV canal explant assay performed at somite number between 24 and 27 (S24–27). Each dot represents one explanted embryo. The line represents the average value and standard error. (F) The number of the outgrowing endocardial cells in the AV canal explant assay performed when EMT is no longer induced at somite number between 29 and 34 (S29–34). Each dot represents one explanted embryo. The line represents the average value and standard error. (G) F-actin immunostaining (green) and TOPRO-3 staining (blue) of AV canal explants from *Tie2CreMM* and control embryos at stage S24–27 and S29–34, respectively. Scale bars = 200 μm. (H) Quantitative measurement of cell densities on the serial sections of endocardial cushions at E9.5 and E11.5, respectively. (I, J) Representative images of BrdU labelling (green) (I) and their quantification (J) in endocardial cushions of the E9.5–E11.5 embryos. Scale bar = 100 μm.

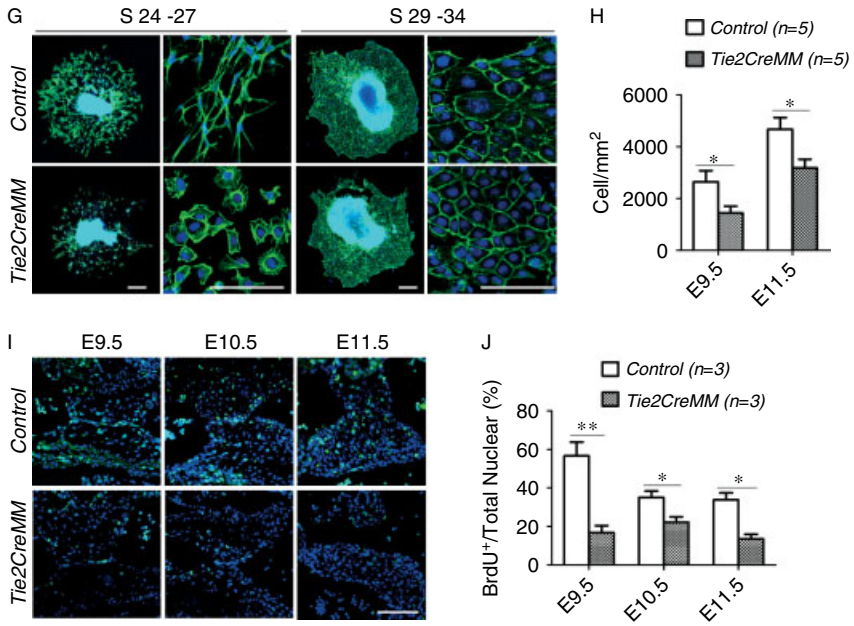

Figure 3. *Continue.*

Cardiac cushion morphogenesis defects in *Tie2Cre;Mdm2*$^{FM/+}$*; Mdm4*$^{+/-}$ (*Tie2CreMM*) mice

Endocardial cells of the AV canal undergo a transient process of EMT at E9.5 to start the formation of AV cushion tissue which is later remodelled to become valves and part of the septum [26]. To assess the potential function of Mdm2 and Mdm4 at the on commitment of EMT, we first checked the expression of EMT-related markers in the AV canal at E9.5. The expression of endomucin, a marker of endothelial lineage, remained high in the endocardium of the *Tie2CreMM* AV canal (Figure 3A), suggesting less commitment to transformation at this stage. In contrast, immunofluorescence revealed reduced expression of vimentin, a mesenchymal marker (Figure 3B), and diminished deposition of fibronectin, an ECM protein (Figure 3C), in the *Tie2CreMM* endocardial cushion. RT-PCR analysis also exhibited a significant down-regulation of *snail*, another EMT marker, as well as *fibronectin* mRNA levels in the E9.5 *Tie2CreMM* heart tubes (Figure 3D).

Culture of AV canal explants on type I collagen gel provides an excellent functional assay to evaluate EMT [31,32]. AV canal explants plated on collagen gels consistently recapitulate the programmed morphogenetic events of EMT *in vivo*, including the inductive effect by the myocardium, and the subsequent endothelial cell migration, activation (delamination of endothelial cells), and transformation into invasive mesenchyme [20,31,33]. To quantitatively measure the regulatory effects of Mdm2 and Mdm4 on EMT for production of invading mesenchymal cells, we first prepared AV canal explant cultures from the *Tie2CreMM* embryos at approximately E9.5 (somite number between 24 and 27) when the EMT process occurs *in vivo*. The *Tie2CreMM* explants showed a significant decrease (50%) in the total number of invading cells in the collagen gel compared with stage matched controls (Figures 3E and 3G, left panel). The majority of cells in the *Tie2CreMM* explants appeared to be rounded with cortical expression of F-actin, compared with the elongated cells with a filamentous pattern of F-actin present in control cells (Figure 3G, left panel); thus, the *Mdm2* and *Mdm4* haplotypes also resulted in a failure of induction of changes in cell morphology normally associated with EMT. At approximately E10.0–E10.5 (somite number between 29 and 34), the endocardial cells in the AV canal are no longer induced to undergo EMT and accordingly, the AV canal explants prepared at this stage display only an expansion of endothelial cell monolayer over the collagen gel without separation and transformation to invading mesenchymal cells [34]. Interestingly, the AV explants isolated at these later developmental stages from the *Tie2CreMM* and control embryos appeared to produce a similar number of outgrowing cells, indicating that the outgrowth (survival and surface migration) of the *Tie2CreMM* endothelial cells *per se* was normal (Figures 3F and 3G, right panel). Taken together, both the immunofluorescence and the AV canal explant results suggested a specific defect in executing the EMT programme in the *Tie2Cre;Mdm2*$^{FM/+}$*; Mdm4*$^{+/-}$ mice.

Next, we quantified the cell density of the endocardial cushions for mesenchymal cell production at E9.5 and found a significant reduction of cellularity in *Tie2CreMM* embryos (Figure 3H), corroborating the *in vitro* results.

After the transient EMT process, the endocardial cushions and subsequent valve primordia undergo growth via cell proliferation [35]. At E11.5, a reduction of cell density in *Tie2CreMM* AV cushions was also observed (Figure 3H). BrdU incorporation was decreased in *Tie2CreMM* cushion mesenchyme

between E9.5 and E11.5, demonstrating that cell proliferation post-EMT was also affected (Figures 3I and 3J). In contrast, cell death was not detected in *Tie2CreMM* cushions, as measured by TUNEL staining at E9.5 (data not shown). The deficiencies on both EMT of endocardial cells and proliferation of mesenchymal cells may account for the AV cushion morphogenesis defect found in *Tie2CreMM* mice.

p53-dependent mechanism affecting cardiac cushion formation and the CHD phenotype in *Tie2Cre;Mdm2$^{FM/+}$; Mdm4$^{+/-}$* mice

To test whether p53 is responsible for the phenotypes exhibited in the *Tie2CreMM* mice, the *p53* null allele was crossed into the *Tie2Cre;Mdm2$^{FM/+}$; Mdm4$^{+/-}$* background to generate *p53$^{+/-}$; Tie2Cre;Mdm2$^{FM/+}$; Mdm4$^{+/-}$* mice. Interestingly, genetic deletion of only one p53 allele was sufficient to rescue the postnatal mortality (Figure 4A), cardiac valvuloseptal defects (Figure 4B), and heart dysfunction (Supplementary Table 3) of the *Tie2CreMM* mice, suggesting that the elevated p53 activity by heterozygous deletion of *Mdm2* and *Mdm4* was possibly responsible for the CHD phenotypes. In addition, the p53-mediated response during AV cushion morphogenesis seemed to be highly sensitive to its dosage.

To determine the p53 functionality during cardiac cushion morphogenesis, immunofluorescence was performed on endocardial cushions from the E9.5

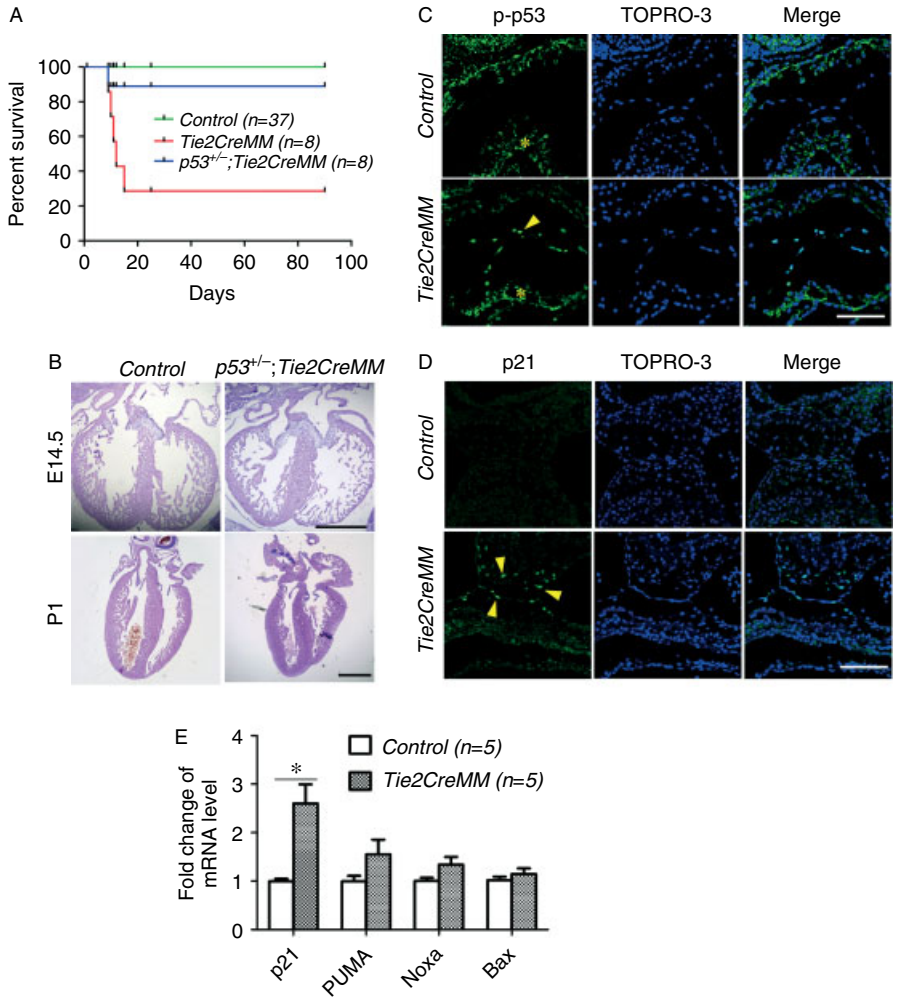

Figure 4. p53-dependent mechanisms affecting cardiac cushion formation and the CHD phenotype in *Tie2Cre;Mdm2$^{FM/+}$; Mdm4$^{+/-}$* mice. (A) Kaplan–Meier survival analysis of *Tie2CreMM*, *p53$^{+/-}$; Tie2CreMM* mice and their littermates. (B) Representative images of *p53$^{+/-}$; Tie2CreMM* hearts revealed no morphological defects. Scale bars = 500 μm. (C, D) Phosphorylated p53 (C) and p21 (D) immunostaining in E9.5 endocardial cushions. Note the strong nuclear p53 and p21 staining in endocardial or mesenchymal cells of the mutant embryo, while absent in the control cushions. Arrowheads indicate positively stained cushion cells. *Non-specific p53 staining in cardiomyocyte. Scale bar = 100 μm. (E) Real-time PCR analysis of the expression of p53 target genes in E9.5 heart tubes. The expression was normalized to the expression of GAPDH and is presented as fold change ± SEM ($n = 5$) relative to the controls. (F) Double immunostaining of β-catenin and phosphorylated p53 (p-p53) in E9.5 endocardial cushions. Note the largely reversed staining pattern between p53 and β-catenin. *Non-specific p53 staining in cardiomyocyte. Scale bar = 100 μm. (G) F-actin immunostaining (green) and TOPRO-3 staining (blue) of AV canal explants from *C57BL/6* embryos at stage S24–27 and S29–34 treated with DMSO or 5 mM Nutlin-3, respectively. Scale bars = 200 μm. (H) Differential interference contrast (DIC) images of AV canal explants from *C57BL/6* embryos treated with DMSO or 10 μM Nutlin-3, respectively. Scale bar = 200 μm. (I) DIC images of AV canal explants from *Tie2Cre;Mdm2$^{FM/FM}$* and control embryos. Scale bar = 200 μm.

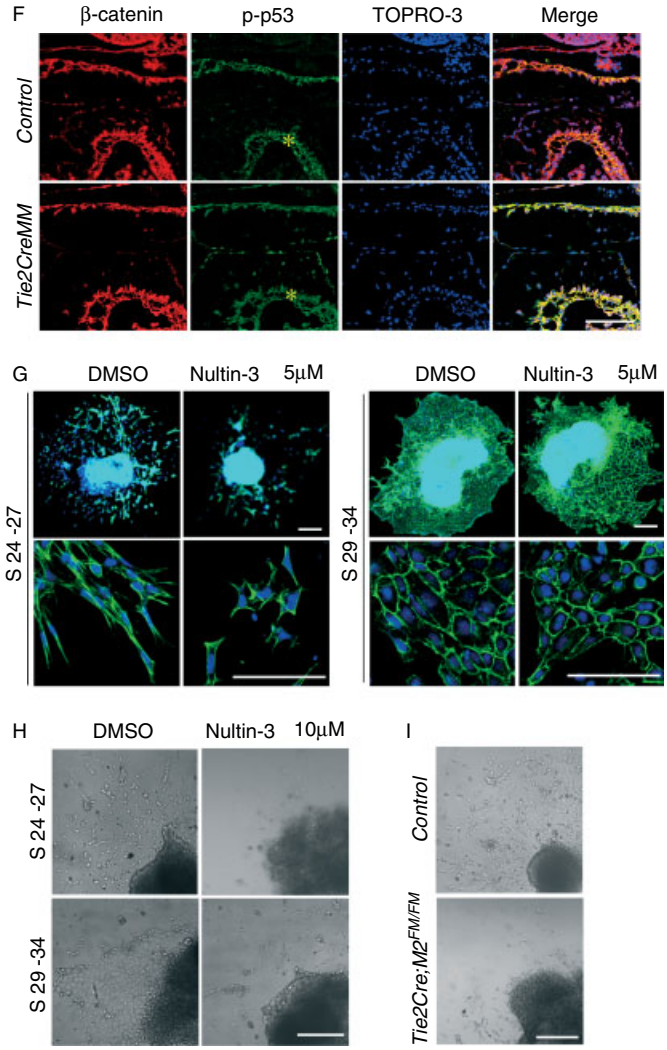

Figure 4. *Continue.*

Table 3. The p53 pathway is involved in CHDs induced by a low dose of X-irradiation on embryos

Time of irradiation	Time of collection	Genotype of offspring	Total	Abnormal	VSD (Mu)	VSD (Me)	ASD	AVSD
E8.5–E9.5	E14.5	$p53^{+/+}$	21	8 (38.1%)	0	4	2	2 (Me)
		$p53^{+/-}$	22	3 (13.6%)*	0	2	1	0
	P1	$p53^{+/+}$	17	6 (35.3%)	0	2	4	0
		$p53^{+/-}$	20	2 (10.0%)	0	0	2	0
E11.5–E12.5	E14.5	$p53^{+/+}$	13	9 (69.2%)	6	0	2	1 (Me)
		$p53^{+/-}$	14	6 (42.8%)	5	0	0	1 (Mu)
	P1	$p53^{+/+}$	6	3 (50.0%)	1	0	2	0
		$p53^{+/-}$	7	2 (28.5%)	1	0	1	0

*C57BL/6 female mice were crossed with $p53^{+/-}$ males. Pregnant females were X-irradiated at 0.3 Gy at the indicated time frames. Numbers in parentheses indicate the percentage of mice affected in the group. Me = membranous; Mu = muscular. * $p < 0.05$. Note the significant decrease of cardiac valvuloseptal defects in $p53^{+/-}$ mice when irradiated at E8.5–E9.5.*

embryos. Phosphorylated p53 staining was detected mostly in the endocardial cushion cells of the *Tie2CreMM* embryo, with no staining in the control embryos (Figure 4C). Immunofluorescence also demonstrated that p21, an important p53 target, was strongly induced in the endocardial cushion cells, with only background staining visible in the control embryos (Figure 4D). We also performed real-time PCR analysis on p53 downstream targets, including *p21*, *Puma, Noxa*, and *Bax* (Figure 4E). While *p21* was up-regulated in the heart tube of the *Tie2CreMM* embryos, *Puma* was only moderately up-regulated, consistent with the fact that we did not observe a significant increase in apoptosis. These results indicated that p53 was transcriptionally active in the endocardial cushions of the *Tie2CreMM* embryos.

To further study the link between p53 activation and EMT deficiency found in the *Tie2CreMM* embryos, double immunofluorescence staining on p53 and the EMT-related marker β-catenin was performed

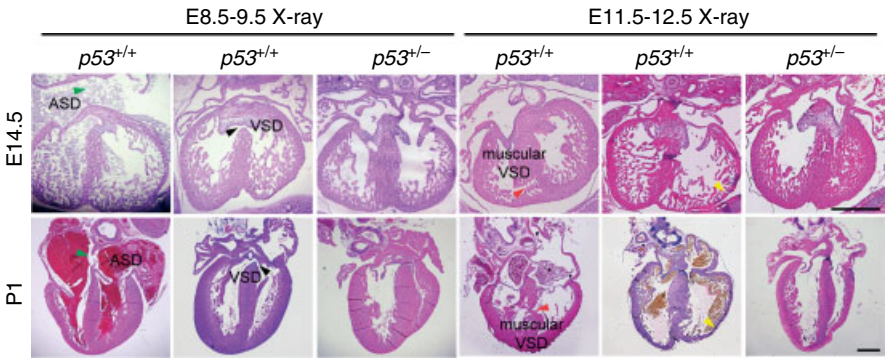

Figure 5. Low-dose X-ray irradiation leads to cardiac valvuloseptal defects in mice. Representative cardiac phenotypes of wild-type and $p53^{+/-}$ mice treated by X-rays at either E8.5–9.5 or E11.5–12.5. Note that wild-type embryos exhibited ASD (green arrowheads) and membranous VSD (black arrowheads) when treated at E8.5–9.5, and muscular VSD (red arrowheads) as well as thin myocardium (yellow arrowheads) when treated at E11.5–12.5. Scale bars = 500 μm.

on the endocardial cushions. β-Catenin expression was decreased, in sharp contrast to the strong p53 staining in the endocardial cells from the *Tie2CreMM* embryo (Figure 4F).

Nutlins were developed as specific Mdm2 antagonists that activate p53 by inhibiting the p53–Mdm2 interaction [36]. It has also been reported that a different dose of Nutlin-3 could elicit differential p53 responses [37]. We then asked whether Nutlin-3 could affect the EMT process in the AV canal explant culture system. Treatment with 5 μM Nutlin-3 significantly reduced mesenchyme cell production in the AV canal explants of the S24–27 stage from the *C57BL/6* mice (Figure 4G, left panel) but did not affect the endothelial outgrowth at the S29–34 stage (Figure 4G, right panel), paralleling the phenotypes seen in the *Tie2CreMM* explant cultures. However, treatment with 10 μM Nutlin-3 completely inhibited not only the mesenchymal cell production from the early-stage explants (Figure 4H, upper panel), similar to the phenotype seen in the *Tie2Cre;Mdm2*$^{FM/FM}$ AV canal explant cultures (Figure 4I), but also the initial outgrowth of endothelial cells from the late-stage explants (Figure 4H, lower panel).

Collectively, these data suggest that mild p53 activation may influence the EMT process during the AV cushion morphogenesis in the *Tie2CreMM* mice.

p53 is involved in X-radiation-induced CHD phenotype in mice

Maternal exposures play a significant role in the development of heart defects in fetuses [24,38]. p53 is stabilized and activated in many stress situations. Among them, X-rays induce p53 protein accumulation in the nuclei of mammalian cells which triggers p53-dependent responses [39]. To determine whether stress-mediated p53 activation could also influence endocardial cushion morphogenesis and the development of CHD phenotypes, $p53^{+/-}$ male mice were crossed with *C57BL/6* females to generate p53 wild-type and heterozygous embryos. Pregnant mice were irradiated by low-dose X-rays (0.3 Gy) between E8.5 and E9. 5 postcorium, right before and when EMT and endocardial cushion morphogenesis were initiated. Hydrocephalus, which has been reported to occur upon a higher dose of X-irradiation [40], was only occasionally found in the treated embryos. However, histological examinations of wild-type embryos at E14.5 and P1 revealed heart defects as the most common phenotype with the irradiation. Cardiac membranous VSD and ASD phenotypes occurred in 36% of the treated embryos, indicating specific valvuloseptal morphogenesis defects (Table 3 and Figure 5, left panel). Intriguingly, exposure of pregnant mice to X-irradiation after the EMT stage at E11.5 and E12.5 promoted a muscular VSD combined with a thin ventricular wall in wild-type embryos instead of the membranous-type defects (Table 3 and Figure 5, right panel), suggesting that X-rays disrupted valvuloseptal morphogenesis during a specific window of time. Importantly, all of these cardiac defects were blunted in $p53^{+/-}$ embryos from the same crosses treated with X-rays (Table 3 and Figure 5), indicating the critical role of the p53 pathway in the pathogenesis of congenital heart defects induced by X-rays.

Discussion

Here we report a new mechanism in which disturbance of p53/Mdm2–Mdm4 signalling can lead to fatal congenital heart defects in mice. Exposure of pregnant mice to a very low-dose of X-rays at the beginning of endocardial cushion morphogenesis also led to p53-dependent heart valvuloseptal developmental defects, establishing a mechanistic link between environmental stresses and the development of CHDs.

p53 is activated by a variety of stress signals, most of which are through relieving the inhibition on p53. As two of the main negative regulators, Mdm2 and Mdm4 play essential roles in repressing p53 during development [5] and tissue homeostasis [41]. Importantly, their regulation is often synergistic, non-overlapping, and dose-dependent, consistent with the facts that p53 activities and responses upon stress are delicately controlled and sensitive to stress strength. In our study, homozygous deletion of *Mdm2* in endothelial cells

led to a disruption of early vascular remodelling and embryonic development, while heterozygous deletions of both *Mdm2* and *Mdm4* bypassed these defects at the early developmental stage and allowed the mice to develop to term, albeit with cardiac valvuloseptal defects. These results demonstrated a drastic difference in the p53 responses as dictated by the nature and dosage of its inhibitors.

The formation of functional cardiac septae and valves from the embryonic endocardial cushions involves a series of morphological events that includes EMT, cushion cellularization and fusion, cell differentiation, and valve-leaflet remodelling. Failure of these processes to occur in a precise temporal sequence often results in clinical endocardial cushion (AV canal) defects, one of the most frequent types of congenital birth defects diagnosed during infancy [18,19,26]. In the present study, we have shown that p53/Mdm2/Mdm4 regulation is critical for normal EMT and post-EMT proliferation essential in septum and valve development. Interestingly, the endocardium in the atrioventricular canal, which is destined to transform into mesenchymal cells, elicits a strong p53 response only after EMT induction in the *Tie2CreMM* embryos and explants since the endocardium itself is intact. The disruption on the EMT process was also recapitulated by treatment of 5 μM Nutlin-3 in the AV canal explant cultures of B6 embryos, while increasing the drug dosage led to inhibition of endothelial cell growth, reminiscent of the phenotype in the *Tie2Cre;M2*$^{FM/FM}$ explants. Lack of proliferation of the post-EMT mesenchymal cells observed in the *Tie2CreMM* embryos should also contribute to the hypocellulaity of the endocardial cushion. These data strongly suggest that cells undergoing EMT or transformed through EMT are hypersensitive to p53 activation. It was reported that p53 and twist, an important EMT inducer, could counteract each other's functions [42]. It is possible that the p53 dosage plays an important role in determining the exact cellular responses. Several more recent studies reported that p53 inhibited EMT through the induction of specific microRNAs that down-regulate EMT inducing genes [43–45]. The induction of these p53 targets in the endocardial cushion cells of the *Tie2CreMM* mice could be one mechanism responsible for the observed phenotypes. Nonetheless, our results clearly identified EMT and post-EMT events as critical targets for a robust p53 response *in vivo*. EMT has been increasingly recognized as a critical step during tumour malignant transformation [46]; thus, our results should also have important implications on understanding the precise role of p53 in suppression of epithelial carcinogenesis.

We developed both a genetic mouse model and environmental (X-ray) induced mouse model of CHDs that shared similar phenotypic characteristics and are both dependent on the p53 dosage, suggesting that p53 activation is the underlying mechanism in the development of CHDs in these mice. Interestingly, ionizing radiation at different developmental windows caused different CHD subtypes. Irradiation at E8.5 and E9.5 led to ASD and membranous VSD in mice, resembling the *Tie2CreMM* phenotype, while irradiation at E11.5 and E12.5 caused ASD and muscular VSD with a thin myocardium, suggesting that the p53 responses during embryonic development may vary in a temporal and tissue-specific manner. Again, these results emphasize the critical window around E9.5 when cushion morphogenesis is initiated and highly susceptible to disturbance mediated through the p53 pathway.

Congenital heart defects are the most prevalent birth defects. Many risk factors are associated with stress signals that could potentially activate the p53 pathway including certain drugs, hypoxia, irradiation, smoke, high blood glucose level, etc [23,24,38]. A better understanding of the complex signalling networks regulating heart development and their interaction with risk factors is necessary to improve the preventative and therapeutic strategies for these defects. We propose that the p53 pathway may provide one of the links between risk factors and the development of CHDs.

Acknowledgment

We wish to thank P Zhou for technical support and H Yang and ZJ Yin for their contribution in initiating the work. We also thank G Lozano for kindly providing the *Mdm2*^{FM} and *Mdm4* mutant mice. This work was supported by the National Key Basic Research Program of China (grants 2006CB943502 and 2010CB945102) and the National Natural Science Foundation of China (grants 30771070 and 30871265).

Author contribution statement

QZ conducted most of the experiments, participated in designing experiments and analysing data, and wrote the manuscript. XH performed the *in vitro* AV canal explant experiments, and LC and CZ helped to perform the experiments. XG and ZY helped in analysing data and editing the manuscript. GL designed and supervised the experiments, evaluated data, and wrote the manuscript.

References

1. Vogelstein B, Lane D, Levine AJ. Surfing the p53 network. *Nature* 2000; **408**: 307.
2. Danilova N, Sakamoto KM, Lin S. Role of p53 family in birth defects: lessons from zebrafish. *Birth Defects Res Part C: Embryo Today: Rev* 2008; **84**: 215–227.
3. Choi J, Donehower LA. p53 in embryonic development: maintaining a fine balance. *Cell Mol Life Sci* 1999; **55**: 38–47.
4. Levine AJ. p53, the cellular gatekeeper for growth and division. *Cell* 1997; **88**: 323–331.
5. Marine JC, Francoz S, Maetens M, *et al*. Keeping p53 in check: essential and synergistic functions of Mdm2 and Mdm4. *Cell Death Differ* 2006; **13**: 927–934.

6. Haupt Y, Maya R, Kazaz A, *et al*. Mdm2 promotes the rapid degradation of p53. *Nature* 1997; **387**: 296–299.
7. Kubbutat MH, Jones SN, Vousden KH. Regulation of p53 stability by Mdm2. *Nature* 1997; **387**: 299–303.
8. Shieh SY, Ikeda M, Taya Y, *et al*. DNA damage-induced phosphorylation of p53 alleviates inhibition by MDM2. *Cell* 1997; **91**: 325–334.
9. Shvarts A, Steegenga WT, Riteco N, *et al*. MDMX: a novel p53-binding protein with some functional properties of MDM2. *EMBO J* 1996; **15**: 5349–5357.
10. Xiong S, Van Pelt CS, Elizondo-Fraire AC, *et al*. Synergistic roles of Mdm2 and Mdm4 for p53 inhibition in central nervous system development. *Proc Natl Acad Sci U S A* 2006; **103**: 3226–3231.
11. Francoz S, Froment P, Bogaerts S, *et al*. Mdm4 and Mdm2 cooperate to inhibit p53 activity in proliferating and quiescent cells *in vivo*. *Proc Natl Acad Sci U S A* 2006; **103**: 3232–3237.
12. Grier JD, Xiong S, Elizondo-Fraire AC, *et al*. Tissue-specific differences of p53 inhibition by Mdm2 and Mdm4. *Mol Cell Biol* 2006; **26**: 192–198.
13. Xiong S, Van Pelt CS, Elizondo-Fraire AC, *et al*. Loss of Mdm4 results in p53-dependent dilated cardiomyopathy. *Circulation* 2007; **115**: 2925–2930.
14. Terzian T, Wang Y, Van Pelt CS, *et al*. Haploinsufficiency of Mdm2 and Mdm4 in tumorigenesis and development. *Mol Cell Biol* 2007; **27**: 5479–5485.
15. Hoffman JI, Kaplan S. The incidence of congenital heart disease. *J Am Coll Cardiol* 2002; **39**: 1890–1900.
16. Olson EN, Schneider MD. Sizing up the heart: development redux in disease. *Genes Dev* 2003; **17**: 1937–1956.
17. Boneva RS, Botto LD, Moore CA, *et al*. Mortality associated with congenital heart defects in the United States: trends and racial disparities, 1979–1997. *Circulation* 2001; **103**: 2376–2381.
18. Wolf M, Basson CT. The molecular genetics of congenital heart disease: a review of recent developments. *Curr Opin Cardiol* 2010; **25**: 192–197.
19. Bruneau BG. The developmental genetics of congenital heart disease. *Nature* 2008; **451**: 943–948.
20. Eisenberg LM, Markwald RR. Molecular regulation of atrioventricular valvuloseptal morphogenesis. *Circ Res* 1995; **77**: 1–6.
21. Olson EN, Srivastava D. Molecular pathways controlling heart development. *Science* 1996; **272**: 671.
22. Pierpont ME, Basson CT, Benson DW, *et al*. Genetic basis for congenital heart defects: current knowledge: a scientific statement from the American Heart Association Congenital Cardiac Defects Committee, Council on Cardiovascular Disease in the Young: endorsed by the American Academy of Pediatrics. *Circulation* 2007; **115**: 3015–3038.
23. Botto L, Correa A. Decreasing the burden of congenital heart anomalies: an epidemiologic evaluation of risk factors and survival. *Prog Pediatr Cardiol* 2003; **18**: 111–121.
24. Jenkins KJ, Correa A, Feinstein JA, *et al*. Noninherited risk factors and congenital cardiovascular defects: current knowledge: a scientific statement from the American Heart Association Council on Cardiovascular Disease in the Young: endorsed by the American Academy of Pediatrics. *Circulation* 2007; **115**: 2995–3014.
25. Nora JJ, Nora AH. The evolution of specific genetic and environmental counseling in congenital heart diseases. *Circulation* 1978; **57**: 205–213.
26. Butcher JT, Markwald RR. Valvulogenesis: the moving target. *Philos Trans R Soc London Ser B Biol Sci* 2007; **362**: 1489–1503.
27. Soriano P. Generalized lacZ expression with the ROSA26 Cre reporter strain. *Nature Genet* 1999; **21**: 70–71.
28. Jacks T, Remington L, Williams BO, *et al*. Tumor spectrum analysis in p53-mutant mice. *Curr Biol* 1994; **4**: 1–7.
29. Kisanuki YY, Hammer RE, Miyazaki J, *et al*. Tie2-Cre transgenic mice: a new model for endothelial cell-lineage analysis *in vivo*. *Dev Biol* 2001; **230**: 230–242.
30. Grier JD, Yan W, Lozano G. Conditional allele of mdm2 which encodes a p53 inhibitor. *Genesis* 2002; **32**: 145–147.
31. Runyan RB, Markwald RR. Invasion of mesenchyme into three-dimensional collagen gels: a regional and temporal analysis of interaction in embryonic heart tissue. *Dev Biol* 1983; **95**: 108–114.
32. Luna-Zurita L, Prados B, Grego-Bessa J, *et al*. Integration of a Notch-dependent mesenchymal gene program and Bmp2-driven cell invasiveness regulates murine cardiac valve formation. *J Clin Invest* 2010; **120**: 3493–3507.
33. Markwald RR, Fitzharris TP, Bolender DL, *et al*. Structural analysis of cell : matrix association during the morphogenesis of atrioventricular cushion tissue. *Dev Biol* 1979; **69**: 634–654.
34. Camenisch TD, Molin DG, Person A, *et al*. Temporal and distinct TGFbeta ligand requirements during mouse and avian endocardial cushion morphogenesis. *Dev Biol* 2002; **248**: 170–181.
35. Sugi Y, Ito N, Szebenyi G, *et al*. Fibroblast growth factor (FGF)-4 can induce proliferation of cardiac cushion mesenchymal cells during early valve leaflet formation. *Dev Biol* 2003; **258**: 252–263.
36. Vassilev LT, Vu BT, Graves B, *et al*. In vivo activation of the p53 pathway by small-molecule antagonists of MDM2. *Science* 2004; **303**: 844–848.
37. Wade M, Rodewald LW, Espinosa JM, *et al*. BH3 activation blocks Hdmx suppression of apoptosis and cooperates with Nutlin to induce cell death. *Cell Cycle* 2008; **7**: 1973–1982.
38. Mone SM, Gillman MW, Miller TL, *et al*. Effects of environmental exposures on the cardiovascular system: prenatal period through adolescence. *Pediatrics* 2004; **113**: 1058.
39. Aubrecht J, Secretan MB, Bishop AJ, *et al*. Involvement of p53 in X-ray induced intrachromosomal recombination in mice. *Carcinogenesis* 1999; **20**: 2229–2236.
40. Aolad HM, Inouye M, Darmanto W, *et al*. Hydrocephalus in mice following X-irradiation at early gestational stage: possibly due to persistent deceleration of cell proliferation. *J Radiat Res (Tokyo)* 2000; **41**: 213–226.
41. Ringshausen I, O'Shea CC, Finch AJ, *et al*. Mdm2 is critically and continuously required to suppress lethal p53 activity *in vivo*. *Cancer Cell* 2006; **10**: 501–514.
42. Shiota M, Izumi H, Onitsuka T, *et al*. Twist and p53 reciprocally regulate target genes via direct interaction. *Oncogene* 2008; **27**: 5543–5553.
43. Chang CJ, Chao CH, Xia W, *et al*. p53 regulates epithelial–mesenchymal transition and stem cell properties through modulating miRNAs. *Nature Cell Biol* 2011; **13**: 1467.
44. Kim NH, Kim HS, Li XY, *et al*. A p53/miRNA-34 axis regulates Snail1-dependent cancer cell epithelial–mesenchymal transition. *J Cell Biol* 2011; **195**: 417–433.
45. Kim T, Veronese A, Pichiorri F, *et al*. p53 regulates epithelial–mesenchymal transition through microRNAs targeting ZEB1 and ZEB2. *J Exp Med* 2011; **208**: 875–883.
46. Thiery JP, Acloque H, Huang RY, *et al*. Epithelial–mesenchymal transitions in development and disease. *Cell* 2009; **139**: 871–890.

SUPPORTING INFORMATION ON THE INTERNET

The following supporting information may be found in the online version of this article.

Table S1. DNA sequences of the primers for the Q-PCR experiments.

Table S2. Genotypic and phenotypic analysis of embryos from *Tie2Cre;Mdm2*$^{FM/+}$ × *Mdm2*$^{FM/FM}$ inter-crosses.

Table S3. Echocardiographic measurements of *p53*$^{+/-}$*; Tie2Cre; Mdm2*$^{FM/+}$*; Mdm4*$^{+/-}$ mice and their littermates.

Figure S1. Tie2 Cre mediated recombination in *Tie2Cre;Mdm2*$^{FM/+}$*; Mdm4*$^{+/-}$ mice.

Figure S2. *Tie2Cre;Mdm2*$^{FM/+}$; *Mdm4*$^{+/-}$ embryos exhibited normal vascular plexus and endocardium formation.

Figure S3. Normal haematopoiesis in the *Tie2Cre;Mdm2*$^{FM/+}$; *Mdm4*$^{+/-}$ mice.